RSC Advances

ROYAL SOCIETY OF CHEMISTRY

www.rsc.org/advances

Nanostructural morphology master-regulated the cell capture efficiency of multivalent aptamers

Liping Xie,[§] Hao Cheng,[†] Hao Qi,[#,⊥] Tongzhou Wang,[†] Hui Zhao,[†] Guoliang Huang,[†] and Yanan Du,[*,†,‡]

[†]Department of Biomedical Engineering, School of Medicine, Tsinghua University, Beijing 100084, China.

[‡]Collaborative Innovation Center for Diagnosis and Treatment of Infectious Diseases, Hangzhou, 310003, China.

[§]College of Life and Health Science, Northeastern University, Shenyang 110819, China.

[#]Key Laboratory of Systems Bioengineering, Ministry of Education (Tianjin University), Tianjin, 300072, China.

[⊥]School of Chemical Engineering and Technology, Tianjin University, Tianjin, 300072, China

* Corresponding author

Fax: +86-10-62773380;

Tel: +86-10-62781691;

E-mail: duyanan@tsinghua.edu.cn

Cells isolation from biological samples is crucial in not only basic research, but also clinical diagnostics. However, there are only a limited number of high-affinity ligands such as antibodies commercially available for cell isolation. Aptamer provides alternative option as affinitive ligand with satisfactory stability and low cost. Unfortunately, only aptamers for certain targets can be screened out and modified to achieve high affinity and specificity. Rolling circle amplification (RCA) of a particular aptamer has been shown to improve its binding affinity to targets due to tandem effect by producing long repeating aptamer sequences. However, the improved binding affinity of the amplified multivalent aptamer could only be achieved within a certain length which would decrease after a threshold amplification length or repeating numbers. Herein, we investigated the effect of nanostructural features of the multivalent aptamer produced by RCA on the cell enrichment efficiency for the first time. The RCA-amplified multivalent aptamer tended to intertwine into micro-scale coils, resulting in decreased effective binding sites and lower enrichment efficiency (5.29%) of the target cells. In contrast, the multivalent aptamer could be stretched into nano-strands by heat-activation exposing more effective binding sites which could increase the cell enrichment efficiency up to 86%. The stretched multivalent aptamer as an ultra affinity agent, provide a powerful tool for high efficient cell capture and separation in personalized disease diagnosis and cell-based research.

1. Introduction

Separation of cells from biological samples is a vital procedure in cell-based basic research (e.g. cell biology,[1] regenerative medicine[2], or clinical diagnostics.[3]) Current methods for cell separation (e.g. fluorescence-activated cell sorting, magnetic-activated cell sorting, or affinity columns) heavily rely on affinitive agents which are either labeled on the cells or conjugated on

the physical substrate for cellular capture. However, most high-affinity agents for cell separation are based on antibodies which are only available for limited protein targets.

Aptamers are oligonucleotides that bind specifically to targets (e.g. protein, small molecules or cells) by unique three-dimensional conformations formed through interactions with targets.[4, 5] Due to their high stability and economical synthesis procedure,[6-9] aptamers have been utilized as affinity agents for various types of targets including cells. Unfortunately, the affinity of most aptamers is not high enough to be comparable to antibodies. It had been proved that dimerization of monovalent aptamers could effectively improve their affinities for the targets.[10, 11] Zhao et al applied rolling circle amplification (RCA) to generate multivalent aptamers as 3D network for cell isolation,[12] which significantly enhanced the capture efficiency as compared with monovalent aptamers and antibodies. RCA is an isothermal enzymatic polymerization technique,[13-15] which can generate long single-strand DNA (ssDNA) with tens to hundreds of tandem repeats of complementary sequence to the circular template oligonucleotide.[16, 17] Since it was discovered in the mid-1990s,[18] RCA has been widely used in genomics, diagnosis and biosensing[13, 14, 19] for signal amplification in gene[20] or protein detection.[21] Various RCA applications have also been developed for the production of repeated DNAzymes and DNA aptamers with repetitive binding motifs as detection platforms for small molecules[22] and proteins.[23]

In the work done by Zhao et al., the cell capture efficiency decreased when RCA reaction was extended beyond 60 min[12]. It was surprising and unexplained why longer reaction time or more aptamer repeats did not result in higher capture efficiency. Here, we hypothesize that the nanostructural morphology of multivalent aptamer is a determining factor for cell capture efficiency that can be controlled to fully release the binding affinity to cells. RCA products were

previously visualized either by atomic force microscopy or fluorescence microscopy, which turned to be chains with many micrometers in length.[23-25] This long ssDNA molecule tended to collapses into a micro-coil.[26-30] As far as we known, there was no report on how the morphology of the multivalent binding motifs amplified by RCA affected the cell enrichment efficiency.

We chose Ramos cell line, a widely used model cell line for Burkitt's lymphoma research, as target cell. The scheme of the multivalent aptamer-mediated cell capture was shown in Figure 1. We hypothesized that the morphology of the RCA-amplified multivalent aptamer would greatly affect cell capture efficiency. In particular, the stretched multivalent aptamer could provide rich effective binding sites to improve the cell capture efficiency. It could be widely applied into high efficient enrichment of physio/pathologically relevant cells (e.g. Ramos cells or circulating cancer/stem cells) for future medical diagnosis and treatment.

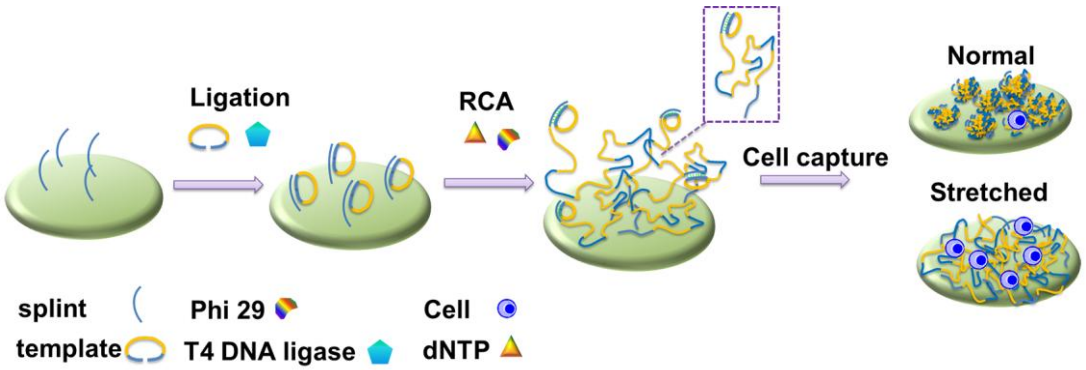

Figure 1. Schematic of multivalent aptamers with different nanostructural morphologies (condensed and stretched) for cell capture.

2. Materials and methods

2.1. Materials

Poly(ethylene glycol) diacrylate (PEGDA) (MW 4000) was purchased from Monomer Polymer & Dajac Labs (Pennsylvania, USA). Octadecyltrichlorosilane (OTS), 3-(trimethoxysilyl)propyl

methacrylate (TMSPMA), ammonium persulfate (APS) and N.N.N'.N'.-tetramethylethylenediamine (TEMED) were purchased from Sigma-Aldrich (St. Louis, USA). N-acryloxysuccinimide and ethanolamine was bought from J&K (Beijing, China). Phosphate buffer was prepared with 137 mM NaCl, 2.7 mM KCl, 10 mM $Na_2HPO_4 \cdot 12H_2O$, 2 mM KH_2PO_4. Ramos (B lymphocyte, human Burkitt's lymphoma) and HL-60 (early promyelocytic acute leukemia cells) were obtained from China Infrastruture of Cell Line Resources (Beijing, China). T4 DNA ligase was obtained from TaKaRa (Shiga, Japan). The phi29 reagent set was purchased from Epi Centre (Madison, U.S.A.). SYBR Green I and SYBR Green II were brought from Biohao (Beijing, China). Oligoncleotides (showed in table S1) were synthesized from the Sangon Biotech Co. Ltd. (Shanghai, China) and purified by high performance liquid chromatography. All aqueous solutions were prepared with deionized water (18 MΩ·cm). All other reagents were purchased from Sigma-Aldrich unless otherwise indicated.

2.2. Characterization of RCA products

Fluorescence stained samples were observed using Nikon EclispseTi-S microscope (Tokyo, Japan). Fluorescent intensity was recorded with a Spectra Max M5 microplate reader with Softmax® Pro Software (Molecular Devices Corporation, USA). Leica Microsystems GmbH (Wetzlar, Germany) was used to characterize the RCA-products array on silica chip. Nano Drop 2000 UV-Vis Spectrophotometer (Thermo, USA) was used to measure the ssDNA contents of the RCA products.

2.3. Cell Culture

Ramos and HL-60 cells were cultured in RPMI 1640 medium with 10% fetal bovine serum (FBS) and 100 IU/mL penicillin streptomycin. The FBS for Ramos was heated to inactivate fetal

bovine serum. The cells were maintained at 37 °C in a humidified atmosphere (95% air and 5% CO_2). The cancer cell densities were determined by using a hemocytometer.

2.4. RCA Reaction in solution and gel electrophoresis

The splint and circular template mixed in 16 μL RCA reaction buffer was first annealed together by heating up to 90 ^oC for 5 min, and then cooled down for 20 min at room temperature. Subsequently, 1 μL T4 DNA ligase, 1 μL ATP and 2 μL T4 ligation buffer was added into the mix, followed by incubation in 22 ^oC for 4 h to prepare for circular template. In order to optimize phi29 polymerase to reduce cost, different concentrations of phi29 polymerase was added. RCA components including phi29 polymerase, 0.625 mM dNTPs, 6.25 mM DTT, 40 mM Tril-HCl, 50 mM KCl, 10 mM $MgCl_2$, and 5 mM $(NH_4)_2SO_4$ were added to 4 μL circular template solution. RCA reaction was carried out at 30 ℃ for a certain time. We characterized the size of the products by 2 % agarose gel electrophoresis. The final products of RCA were analyzed by fluorescence, TEM, and DNA absorption at 260 nm.

2.5. Preparation of PEG-hydrogel on glass

PEGDA4000 was chosen as cell capture substrate considering its biocompatibility and low non-specific adsorption, and N-acryloxysuccinimide was used as a bio-ligand for amine-modified DNA. Glass substrates were treated with 1% TMSPMA for 10 min, and baked at 60 ℃ for 4 h. A hydrophobic substrate (OTS-treated glass) was made by a similar procedure. The cleaned glass slides were immersed into an OTS/n-heptane solution for 10 min, then rinsed with ethanol and dried at 60 ℃ for 4 h. To form hydrogel on the glass, 10% (m/v) PEGDA4000 and 1% (m/v) N–acryloxysuccinmide were dissolved in PBS (pH=8.0) thoroughly with vortex. 0.5% (m/v) APS and 0.05% (m/v) TEMED was added into the PEGDA4000 solution on ice, and mixed well. 15 μL of the mixture was dropped onto the TMSPMA coated glass with three repeats, and two

spacer slides were used to keep the hydrogel with a height around 300 μm. Finally, an OTS coated glass slide was put onto the hydrogel solution as a cover slide. After 1 h at room temperature, the OTS slide was uncovered, and the PEGDA4000 hydrogel was washed thoroughly with PBS.

2.6. RCA on the surface of hydrogel

Splint DNA sequence (Splint) / scramble splint DNA sequence (Template_scr) / mono aptamer was diluted in PBS (pH=8.0) with a final concentration of 5 μM. The DNA solution was added onto the hydrogel surface with a ratio of 7.5 μL DNA/15 μL hydrogel, and incubated at 4 ℃ over night. 500 mM ethanolamine was used to block the unreacted group, and the extra ethanolamine was removed by washing with PBS buffer. The native and mono aptamer modified hydrogels were then treated in PBS for further use. As for RCA-hydrogels and fake RCA-hydrogels, 7.5 μL of the 5 μM template solution was added onto one hydrogel and annealed at 60 ℃ for 30 min, then allowed to cool to room temperature. 66 mM Tris-HCl, 6.6 mM $MgCl_2$, 10 mM DTT, 1 mM ATP and 40 U/μL T4 DNA ligase were mixed thoroughly and added onto one hydrogel. The ligation reaction took 4 h under room temperature. Finally each hydrogel was added with 30 μL RCA reaction mix (containing 5 U/μL phi29 polymerase, 0.625 mM dNTPs, 6.25 mM DTT, 40 mM Tril-HCl, 50 mM KCl, 10 mM $MgCl_2$, and 5 mM $(NH_4)_2SO_4$). The RCA reaction was stopped by washing with PBS. For the fake RCA-hydrogel, the procedure was the same except that no phi29 enzyme was added to RCA reaction.

2.7. Probe staining and dissociation

After surface modification, the desired concentration of ssDNA probes with 6-FAM fluorescein at 5' end was used to stain the hydrogel. First the probes were annealed on the hydrogel at 60 °C for 30 min, then, allowed to cool to room temperature, and then incubated at room temperature

for 15 min. Hydrogel was washed with PBS thoroughly to remove unspecific DNA probes, and was cut into pieces before transferred into a tube. A desired volume of dissociation buffer (3.5 M urea, 10 mM EDTA, 0.02% Tween 20, and 40 mM Tris-HCl with pH=8.0) was added into the tube. The probe dissociation experiment was performed at 90 °C, and after 15 min, the supernatant was transferred into the 384 standard well for microplate reader readout at 495/520 nm excitation and emission wavelength.

2.8. RCA products measured by the hyper-spectral imaging system

The substrate used for thickness measure was a small (3 mm × 5 mm) silicon chip with a thin epoxy-modified SiO_2 film which was visualized by the hyper-spectral imaging system. The splint was re-suspended at a concentration of 5 μM in 50% dimethyl sulfoxide (DMSO) and printed by SmartArrayer^{TM}-48 Microarray Spotter (Capital Bio). The spot diameter was approximately 50 μm at 200 μm center-to-center spacing. The following RCA reaction was the same as the one on hydrogel. A part of the multivalent aptamers produced by RCA was stretched by heat-activation, marked as stretched sample. The other part without any treatment was marked as normal sample. In order to keep the morphologies of the multivalent aptamers, the stretched and normal samples were put on liquid nitrogen, then dried by lyophilization.

2.9. Cell capture

Both target cells (Ramos) and control cells (HL-60) were centrifuged and re-suspended in the medium to a desired concentration (2×10^5 cells/ml). The RCA modified and mono aptamer modified hydrogels were both activated at 90 ℃ for 5 min in a humidified petri-dish, and then stored at 4 ℃ before use. The cells were loaded directly onto the hydrogel and incubated on ice for 45 min. After incubation, unbound cells were washed off by PBS buffer. The capture cells were taken under the microscope, and cell numbers were calculated by ImageJ.

3. Results and discussion

3.1 Long rolling circle amplification products

A padlock oligonucleotide probe was designed for RCA reaction. The padlock template composed of a complementary sequence of previously selected aptamer[31-33](Figure 2a) specific to bind Ramos and a spacer sequence. The template (Figure 2b) contains two target complementary segments to a splint at opposite ends. Upon hybridization to the splint sequence, the 5' and 3' end was brought in contact to form a circular oligonucleotide in the presence of T4 DNA ligase. By careful theoretical design, the RCA products consisting of multivalent aptamer units would not form intra-molecular structure (Figure 2c, 2d, 2e). To verify the successful circularization of the RCA template, 2% agarose gel electrophoresis was performed. Figure S1 showed the result of the gel electrophoresis, with the conformational change of DNA resulting in difference in their migration rates (lane 1 and lane 3 in Figure S1). The results of the gel electrophoresis confirmed the successful circularization of the RCA template. Lane 4 was the RCA products, which were long ssDNA molecules with extremely low mobility. These results demonstrated the successful amplification of the RCA products. Phi29 DNA polymerase is stable, and with linear reaction kinetics at 30℃ for over 12 h.[34] This isothermal enzyme combines the qualities of high processivity with good strand displacement properties, and does not need additional proteins when applied in DNA replication *in vitro*.[35] To minimize the usage of phi29 polymerase and keep RCA performance, the concentration of phi29 DNA polymerase was optimized. The RCA products amplified by different concentrations of phi29 DNA polymerase with varied reaction time were analyzed by gel electrophoresis, which was shown in Figure S2. The amounts of RCA products could be simply tuned by the RCA reaction time and the concentration of phi29 DNA polymerase. When the phi29 DNA polymerase turned to 5

U/μL, the RCA products could be still produced, which was chosen as the reaction concentration in the following experiment.

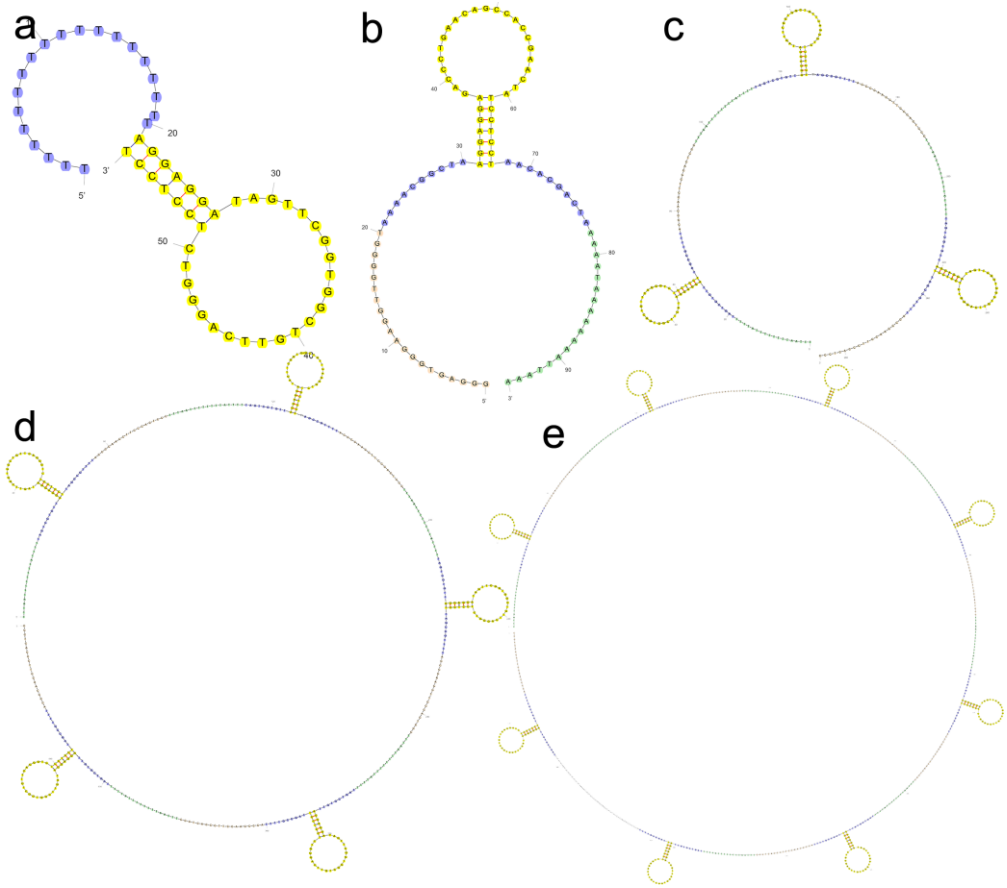

Figure 2. Simulation of secondary structures of ssDNA sequences. (a) mono aptamer, (b) template sequence, (c) 3 repeats of RCA products, (e) 5 repeats of RCA products, (f) 8 repeats of RCA products. The color of the ssDNA sequences indicate the functional sequences accordingly, with aptamer /corresponding complement sequences in yellow, spacer sequences in blue, and the splints in green and orange.

3.2. Morphology of the RCA products

The RCA products turned to be chains of several micrometers in length. These long products tended to collapse into miro-spheres. In order to investigate the intra-molecular and inter-molecular interaction of the RCA products, we investigated two states of RCA products stained

with SYBR Green I, which could preferentially bind double stranded DNA or dimmers[36]with significant fluorescence over single stranded DNA. SYBR Green I is therefore an ideal staining for detecting double stranded DNA (dsDNA) in complex sample mixed with ssDNA or RNA.[37] The RCA products were divided into two parts. One part was kept at 4 ℃ and marked as normal sample. The other part was activated at 90 ℃ for 5 min before kept at 4 ℃, and marked as stretched sample. The two parts were stained with SYBR Green I on ice for 15 min. The fluorescence images of the normal and the stretched samples were captured under the same condition for analyzing the interaction of the multivalent aptamers (Figure 3). As the RCA reaction time increased (from 10 min to 720 min), the fluorescence intensity of the normal multivalent aptamers stained with SYBR Green I was increased significantly, and some fluorescent micro-coils appeared in the 270 min, 540 min (Figure S3) and 720 min samples (Figure 3a). These phenomena indicated that the intra-molecular and inter-molecular interaction of the multivalent aptamers was significantly enhanced as the RCA reaction time increased. Interestingly, the fluorescence intensity of the stretched samples was significantly lower than the corresponding normal samples, which demonstrated that the tangling of the multivalent aptamers was decreased, and more effective binding sites were released. Some green fluorescence appeared in the stretched samples (Figure 3), since SYBR Green I could bind some base-paired units of stem-loops, bulges, pseudo-knots. To quantify the fluorescence intensity, we used microplate reader to measure the specific intensity. As shown in Figure 3b, the results were in accordance with the fluorescence images. There were no significant differences between the stretched samples. However, the fluorescence intensity of the normal samples distinctly increased with the extension of RCA reaction time. In the 10 min and 30 min sample, the intensity between the stretched and normal samples were nearly the same. As the RCA reaction

time increased, the differences were conspicuous (Figure 3c). The tangling of the RCA products was aggravated as the RCA reaction time increasing. The normal multivalent aptamers tended to aggregate with more effective binding sites buried inside. While, the stretched samples could release more ssDNA, reducing tangling of the multivalent aptamers. To further verify this phenomenon, we tested change in the amount of ssDNA between the two states of morphologies. It is well-known that the absorption at 260 nm is different between the ssDNA and dsDNA, and the absorption intensity at 260 nm of the ssDNA is larger than dsDNA. By using the Nanodrop, we got the absorption changes between the normal and corresponding stretched samples at 260 nm. The absorption changes at 260 nm increased with the RCA reaction time (Figure S4). After being stretched, more ssDNA could be released from the micro-coils, exposing much more binding sites. To explore the morphology of RCA products on 2D hydrogel for cell capture, we performed the RCA reaction on 2D PEG-hydrogel, and got the florescence images of RCA products stained with SYBR Green I (Figure S5). The trend of change was similar to the RCA products in solution.

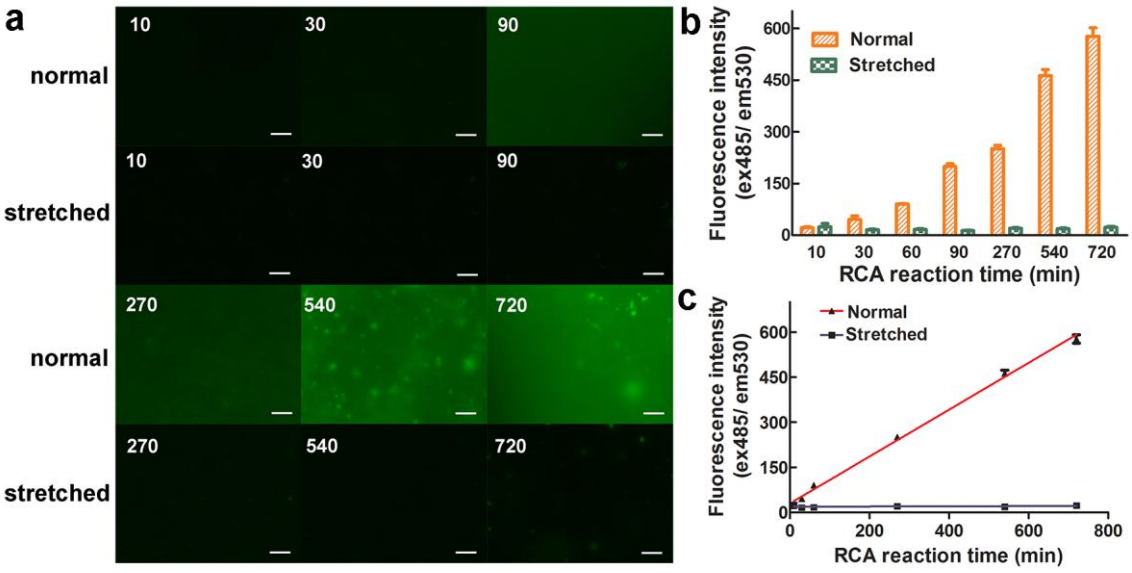

Figure 3. RCA amplified multivalent aptamers with different reaction time stained with SYBR Green I in solution. (a) Fluorescence images. (b) and (c) are the fluorescence quantitative analysis. Scale bars are 50 μm.

We further characterized the thickness of the RCA products with two states of morphologies, by using the home-made hyper-spectral imaging system.[38] As showed in Figure 4a, the top three rows were the RCA products, and the last three rows were the control group immobilized with scramble splints which could not be amplified by RCA. The RCA products were obviously brighter than the control group, which verified that the RCA products were successfully amplified. The stretched samples were flexible and looked smaller when measured by the hyper-spectral imaging system. The thickness of normal RCA products was about 20 nm (Figure 4b, d). In contrast, the thickness of the stretched RCA was significantly reduced, which was about 7 nm (Figure 4c, e), and the area of the RCA products was reduced. In order to verify that heat activation could make the RCA products stretch, and prevent RCA products from aggregation, we further obtained the TEM images of the two states of the multivalent aptamers. As shown in Figure 5, the normal samples aggregated into micro-coils (Figure 5a,b). The stretched samples presented long single chains (Figure 5c, d). The arrows in Figure 5d indicated long ssDNA chain. Heat activation stretched the micro-coils into a more flattened layer, and released more binding sites, which provided large contact area for interaction with target cells.

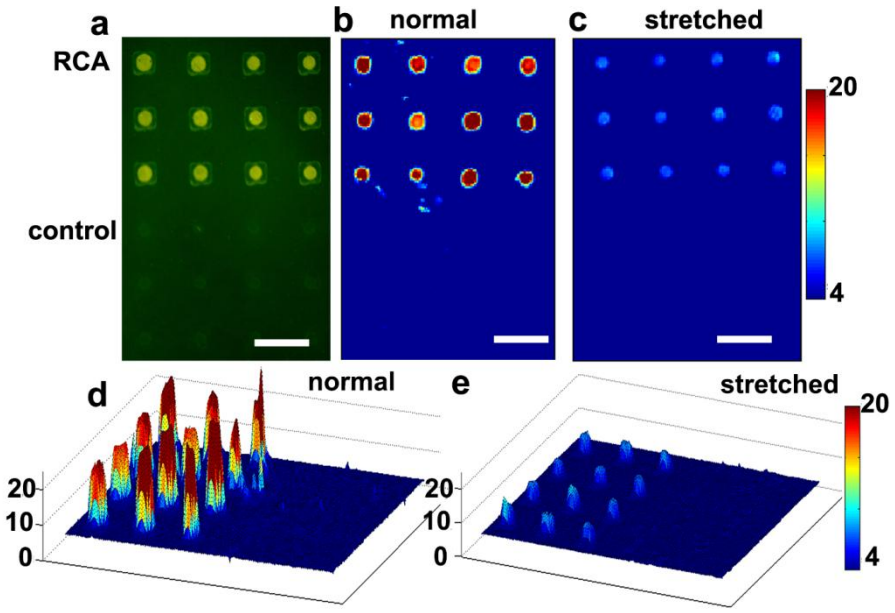

Figure 4. RCA amplified multivalent aptamers with normal and stretched morphologies. (a) Fluorescence images. Thickness of RCA products with normal (b) and stretched (c) morphology in 2D. (d) and (e) are the 3D thickness visualized by hyper-spectral imaging system respectively. Scale bars are 200 μm.

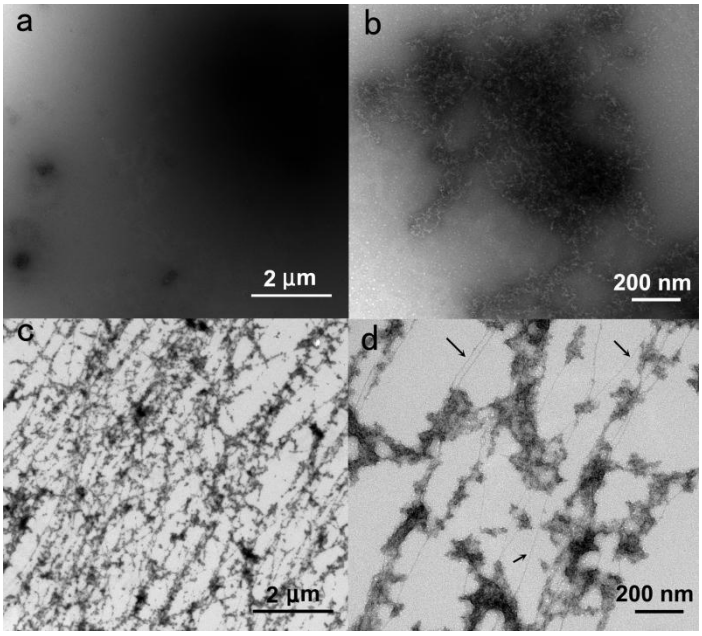

Figure 5. TEM images of multivalent aptamer with normal (a, b) and stretched (c, d) morphologies.

3.3. Cell Enrichment Effciency

To test cell enrichment efficiency of RCA-amplified multivalent aptamers, we performed RCA on PEG-hydrogel. Sequence-specific ssDNA probes with FAM at the 5' end were used to stain the RCA products. The RCA group was much brighter than the mono (aptamer only), the fake (without phi29 DNA polymerase), as well as the native PEG-hydrogel (Figure S6). The quantitative analysis was shown in Figure S6e. The fluorescence intensity of the RCA group was nearly ten times stronger than the mono group. To further investigate the reusability of multivalent aptamer, we eluted the specific probe by 8 M urea, and then restained the RCA-samples. Quantitative analysis shown that the RCA-amplified multivalent aptamer could be reusable at least for 5 times as experimentally proved here. We also characterized the morphology of RCA products on PEG-hydrogel. As shown in Figure S7, the surface of native hydrogel was smooth, and the normal group was much rougher than the native hydrogel. However, the stretched sample was relative smooth to a certain extent, which demonstrated that heat-activation could stretch the micro-coils into more flattened nanostructural morphology, releasing more effective binding sites.

To investigate the effect of multivalent aptamer morphology on the cell enrichment, we applied the two states of multivalent aptamers conjugated on PEG-hydrogel with different RCA reaction time to enrich target cells (Ramos). As shown in Figure S8, cell capture efficiency of the normal multivalent aptamers increased with RCA reaction time until the RCA time reached 90 min achieving 5.29% cell capture efficiency. When the RCA reaction time was over 90 min, the cell capture efficiency significantly decreased. In contrast, the cell capture efficiency of the stretched multivalent aptamers dramatically increased with RCA reaction time, showing a linear relationship with RCA reaction time (Figure 6). When the RCA reaction time reached to 960 min, the cell capture efficiency significantly increased up to 86%, about 16 fold higher than the

cell capture efficiency of the normal multivalent aptamers. The morphology of the RCA-amplified multivalent aptamer played an important role on the affinity for target cells. The bigger size and lower diffusion rate of cells would reduce contact probability with the multivalent aptamers. The RCA-amplified multivalent aptamers tended to intertwine into micro-coils, resulting in decreased effective binding sites and lower target cell enrichment efficiency. While the multivalent aptamer subjected to heat-activation could be stretched into nano-strands, exposing more effective binding sites which increased the cell enrichment efficiency up to 86%. In addition, it was likely due to the nanostructure formed by the stretched multivalent aptamer resulting in larger contact area between the cells and the PEG-hydrogel surface compared to the micro-coils substrate.

We further applied the stretched RCA amplified for 960 min to test the effect of the cell enrichment. The multivalent aptamer could differentiate the target (Ramos) from the control cell (HL-60) (Figure S9). The cell capture efficiency of the native, fake RCA, and scramble RCA were negligible. As for the stretched multivalent aptamer group, the cell capture efficiency was significantly improved. We also compared the cell capture efficiency with different concentrations of aptamer (from 5 μM to 250 μM). As the aptamer concentration increased, the cell capture efficiency increased as well. However, even the concentration of aptamer increased to 250 μM, the cell capture efficiency was still much lower than the stretched multivalent aptamer group. We optimized the temperature of cell capture as well. As shown from Figure S10, the cell capture efficiency decreased as the temperature of cell capture increased, which could be explained that the aptamer targeting to Ramos cell exhibits a best affinity at 4 ℃.[31, 32]

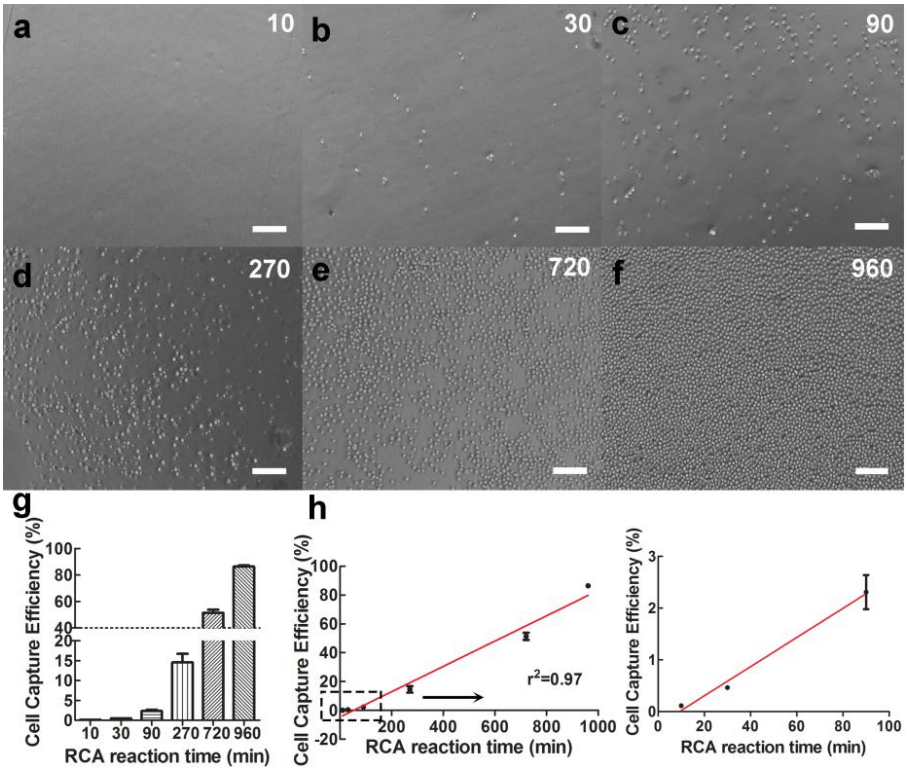

Figure 6. Cell capture efficiency by the stretched multivalent aptamer with various RCA reaction time. (a) 10 min, (b) 30 min, (c) 90 min, (d) 270 min, (e) 720 min, (f) 960 min, (g) and (h) are the statistical analysis of cell capture efficiency. Scale bars are100 μm.

4. Conclusions

In summary, we investigated the nanostructural features of the multivalent aptamers produced by RCA on the cell enrichment efficiency. The long multivalent aptamer in ambient conditions tended to intertwine into coils, resulting in decreased effective binding sites and lower enrichment efficiency (5.29%) of the target cells. In contrast, the stretched multivalent aptamer by heat-activation could expose much more effective binding sites, and increased the cell enrichment efficiency up to 86%. Nanostructural morphology formed by stretched multivalent aptamers regulated target cell capture efficiency, which formed higher contact area with target cells, resulting in higher cell capture efficiency. The stretched multivalent aptamers provided a

powerful tool for personalized disease diagnosis based on quantification of the enriched circulating cells from body fluids.

Declaration of interest statement

No potential conflicts of interest were disclosed.

Acknowledgements

We thank all du-lab members for general assistance. This work is financially supported by the Natural Science Foundation of China (81171474, 51273106, 81327005, 51461165302) and the Beijing Municipal Natural Science Foundation (157142090).

Notes and references

1 A. Kumar, I. Yu and G. Bo, *Cell Separation: Fundamentals Analytical and Preparative Methods*, Springer-Verlag, Berlin Heidelberg, 2007.

2 P. Bianco and P. G. Robey, *Nature*, 2001, **414**, 118-121.

3 S. Nagrath, L. V. Sequist, S. Maheswaran, D. W. Bell, D. Irimia, L. Ulkus, M. R. Smith, E. L. Kwak, S. Digumarthy, A. Muzikansky, P. Ryan, U. J. Balis, R. G. Tompkins, D. A. Haber and M. Toner, *Nature*, 2007, **450**, 1235-1239.

4 A. D. Ellington and J. W. Szostak, *Nature*, 1990, **346**, 818-822.

5 R. Nutiu and Y. Li, *Angew. Chem.*, 2005, **117**, 1085-1089.

6 L. Gold, *J Biol Chem*, 1995, **270**, 13581-13584.

7 T. Hermann and D. J. Patel, *Science*, 2000, **287**, 820-825.

8 L. Chen, X. Liu, B. Su, J. Li, L. Jiang, D. Han and S. Wang, *Adv Mater*, 2011, **23**, 4376-4380.

9 S. D. Jayasena, *Clin Chem*, 1999, **45**, 1628-1650.

10 Y. Nonaka, W. Yoshida, K. Abe, S. Ferri, H. Schulze, T. T. Bachmann and K. Ikebukuro, *Anal Chem*, 2012, **85**, 1132-1137.

11 H. Hijiri, T. Ken-ichi, S. Koji and I. Kazunori, *Sensors*, 2008.

12 W. Zhao, C. H. Cui, S. Bose, D. Guo, C. Shen, W. P. Wong, K. Halvorsen, O. C. Farokhzad, G. S. L. Teo, J. A. Phillips, D. M. Dorfman, R. Karnik and J. M. Karp, *Proc. Natl. Acad. Sci.*, 2012, **109**, 19626-19631.

13 P. M. Lizardi, X. Huang, Z. Zhu, P. Bray-Ward, D. C. Thomas and D. C. Ward, *Nat Genet*, 1998, **19**, 225-232.

14 W. Zhao, M. Ali, M. Brook and Y. Li, *Angew. Chem. Int. Ed.*, 2008, **47**, 6330-6337.

15 C. Ding, H. Liu, N. Wang and Z. Wang, *Chem Commun*, 2012, **48**, 5019-5021.

16 S. L. Daubendiek, K. Ryan and E. T. Kool, *J Am Chem Soc*, 1995, **117**, 7818-7819.

17 D. Liu, S. L. Daubendiek, M. A. Zillman, K. Ryan and E. T. Kool, *J Am Chem Soc*, 1996, **118**, 1587-1594.

18 A. Fire and S. Q. Xu, *Proc. Natl. Acad. Sci.*, 1995, **92**, 4641-4645.

19 M. Stougaard, S. Juul, F. F. Andersen and B. R. Knudsen, *Integrative Biology*, 2011, **3**, 982-992.

20 J. Goransson, C. Wahlby, M. Isaksson, W. M. Howell, J. Jarvius and M. Nilsson, *Nucleic Acids Res*, 2009, **37**, e7.

21 L. Yang, C. W. Fung, E. J. Cho and A. D. Ellington, *Anal Chem*, 2007, **79**, 3320-3329.

22 Z. Cheglakov, Y. Weizmann, B. Basnar and I. Willner, *Organic & Biomolecular Chemistry*, 2007, **5**, 223-225.

23 Z. Cheglakov, Y. Weizmann, A. B. Braunschweig, O. I. Wilner and I. Willner, *Angew. Chem. Int. Ed.*, 2008, **47**, 126-130.

24 Z. Deng, Y. Tian, S. Lee, A. E. Ribbe and C. Mao, *Angew. Chem.*, 2005, **117**, 3648-3651.
25 S. Beyer, P. Nickels and F. C. Simmel, *Nano Lett*, 2005, **5**, 719-722.
26 G. A. Blab, T. Schmidt and M. Nilsson, *Anal Chem*, 2003, **76**, 495-498.
27 J. Jarvius, J. Melin, J. Goransson, J. Stenberg, S. Fredriksson, C. Gonzalez-Rey, S. Bertilsson and M. Nilsson, *Nat Meth*, 2006, **3**, 725-727.
28 E. Schopf, N. O. Fischer, Y. Chen and J. B. H. Tok, *Bioorg. Med. Chem. Lett.*, 2008, **18**, 5871-5874.
29 M. Strömberg, J. Göransson, K. Gunnarsson, M. Nilsson, P. Svedlindh and M. Strømme, *Nano Lett*, 2008, **8**, 816-821.
30 J. Melin, J. Jarvius, J. Göransson and M. Nilsson, *Anal Biochem*, 2007, **368**, 230-238.
31 P. R. Mallikaratchy, A. Ruggiero, J. R. Gardner, V. Kuryavyi, W. F. Maguire, M. L. Heaney, M. R. McDevitt, D. J. Patel and D. A. Scheinberg, *Nucleic Acids Res*, 2011, **39**, 2458-2469.
32 P. Mallikaratchy, Z. Tang, S. Kwame, L. Meng, D. Shangguan and W. Tan, *Mol. Cell. Proteomics*, 2007, **6**, 2230-2238.
33 Z. Tang, D. Shangguan, K. Wang, H. Shi, K. Sefah, P. Mallikratchy, H. W. Chen, Y. Li and W. Tan, *Anal Chem*, 2007, **79**, 4900-4907.
34 F. B. Dean, J. R. Nelson, T. L. Giesler and R. S. Lasken, *Genome Res*, 2001, **11**, 1095-1099.
35 L. Blanco, A. Bernad, J. M. Lázaro, G. Martín, C. Garmendia and M. Salas, *J Biol Chem*, 1989, **264**, 8935-8940.
36 K. M. Ririe, R. P. Rasmussen and C. T. Wittwer, *Anal Biochem*, 1997, **245**, 154-160.
37 I. M. Mackay, K. E. Arden and A. Nitsche, *Nucleic Acids Res*, 2002, **30**, 1292-1305.
38 T. Wang, Q. Li, X. Li, S. Zhao, Y. Lu and G. Huang, *Opt Lett*, 2013, **38**, 1524-1526.